


# Development of a Testing Funnel for Identification of Small-Molecule Modulators Targeting Secretin Receptors

SLAS Discovery  
2021, Vol. 26(1) 1–16  
© Society for Laboratory  
Automation and Screening 2020  
DOI: 10.1177/247255220945284  
journals.sagepub.com/home/jbx  


Daniela G. Dengler<sup>1</sup>, Qing Sun<sup>1</sup>, John Holleran<sup>1</sup>, Sirkku Pollari<sup>1</sup>, Jannis Beutel<sup>2</sup>, Brock T. Brown<sup>1</sup>, Aki Shinoki Iwaya<sup>1</sup>, Robert Ardecky<sup>1</sup>, Kaleeckal G. Harikumar<sup>3</sup>, Laurence J. Miller<sup>3</sup>, and Eduard A. Sergienko<sup>1</sup>

## Abstract

The secretin receptor (SCTR), a prototypical class B G protein-coupled receptor (GPCR), exerts its effects mainly by activating G $\alpha$ s proteins upon binding of its endogenous peptide ligand secretin. SCTRs can be found in a variety of tissues and organs across species, including the pancreas, stomach, liver, heart, lung, colon, kidney, and brain. Beyond that, modulation of SCTR-mediated signaling has therapeutic potential for the treatment of multiple diseases, such as heart failure, obesity, and diabetes. However, no ligands other than secretin and its peptide analogs have been described to regulate SCTRs, probably due to inherent challenges in family B GPCR drug discovery. Here we report creation of a testing funnel that allowed targeted detection of SCTR small-molecule activators. Pursuing the strategy to identify positive allosteric modulators (PAMs), we established a unique primary screening assay employing a mixture of three orthosteric stimulators that was compared in a screening campaign testing 12,000 small-molecule compounds. Beyond that, we developed a comprehensive set of secondary assays, such as a radiolabel-free target engagement assay and a NanoBiT (NanoLuc Binary Technology)-based approach to detect  $\beta$ -arrestin-2 recruitment, all feasible in a high-throughput environment as well as capable of profiling ligands and hits regarding their effect on binding and receptor function. This combination of methods enabled the discovery of five promising scaffolds, four of which have been validated and further characterized with respect to their allosteric activities. We propose that our results may serve as starting points for developing the first in vivo active small molecules targeting SCTRs.

## Keywords

high-throughput screening, secretin receptor, positive allosteric modulator, TR-FRET binding, G protein-coupled receptor

## Introduction

In 1902, Bayliss and Starling discovered secretin (Sec-FL [full-length]), a 27-amino acid hormone, in the duodenal mucosa stimulating the secretion of bicarbonate, enzymes, and potassium ions from the pancreas.<sup>1</sup> Sec-FL exerts its physiological effects by activating the secretin receptor (SCTR), which was cloned in 1991 as the first member of the class B family of G protein-coupled receptors (GPCRs).<sup>2</sup> Thus, secretin and its receptor formed the backbone of this highly important family of therapeutic targets, which are crucially involved in hormonal homeostasis.<sup>3</sup> Beyond its secretory effect, Sec-FL is implicated in a number of physiological and pathological conditions involving the heart, lung, liver, brain, and gastrointestinal (GI) system.<sup>4</sup> According to Grossini et al.,<sup>5</sup> intracoronary infusion of secretin in animal models or human patients demonstrated beneficial cardiac responses, such as positive inotropic,

<sup>1</sup>Conrad Prebys Center for Chemical Genomics, Sanford Burnham Prebys Medical Discovery Institute, La Jolla, CA, USA

<sup>2</sup>Department of Chemistry and Pharmacy, Chemikum, Friedrich-Alexander University Erlangen-Nuremberg, Erlangen, Germany

<sup>3</sup>Department of Molecular Pharmacology and Experimental Therapeutics, Mayo Clinic, Scottsdale, AZ, USA

Received April 30, 2020, and in revised form June 24, 2020. Accepted for publication June 29, 2020.

Supplemental material is available online with this article.

### Corresponding Authors:

Daniela G. Dengler, Conrad Prebys Center for Chemical Genomics, Sanford Burnham Prebys Medical Discovery Institute, 10901 N Torrey Pines Rd, La Jolla, CA 92037, USA.

Email: ddengler@sbgpdiscovery.org

Eduard A. Sergienko, Conrad Prebys Center for Chemical Genomics, Sanford Burnham Prebys Medical Discovery Institute, 10901 N Torrey Pines Rd, La Jolla, CA 92037, USA.

Email: esergien@sbgpdiscovery.org

chronotropic, and vasodilating effects, without changing the blood pressure. Furthermore, SCTR has been shown to stimulate meal-induced brown fat thermogenesis resulting in satiation and short-term reduction of food intake.<sup>6</sup> A recent report highlighted elevated postprandial secretin plasma concentrations after Roux-en-Y gastric bypass (RYGB) surgery, which unveiled glucose-sensitive S (secretin) cells in the distal small intestine.<sup>7</sup> In addition, SCTR activation might be of therapeutic value for functional dyspepsia as indicated in a small clinical study in humans.<sup>8</sup> Altogether, modulating SCTR signaling outlines a unique strategy to develop novel therapeutics with potential benefits for the treatment of comorbid conditions, such as obesity, diabetes, abnormal gastric accommodation, and heart failure. However, to date, no ligands other than secretin peptide and closely related analogs have been identified to interact with SCTRs.<sup>9–11</sup> Beyond that, synthetic Sec-FL represents the only clinically utilized SCTR ligand for diagnostic purposes.<sup>12,13</sup> This might be due to the practical clinical limitations of Sec-FL, such as its short half-life (~2–4 min) and the need for intravenous administration.<sup>8</sup> Moreover, the development of potent small-molecule ligands for class B GPCRs remains challenging, likely due to the complex binding mechanism of orthosteric endogenous ligands within the N-domain and the highly open seven-transmembrane region of these receptors.<sup>3,14</sup> Nonetheless, recent diabetes research has led the way by identifying a vast number of small-molecule modulators targeting the glucagon-like peptide-1 receptor (GLP-1R),<sup>15–20</sup> a close relative to the SCTR. Although no orally available GLP-1R drug has been approved for human use,<sup>20</sup> the pace of emerging small-molecule GLP-1R ligands expands drug discovery for class B GPCRs. The quest for ligands that interact via allosteric binding sites contributed largely to this breakthrough. This class of compounds, which binds to structurally distinct receptor pockets, offers an opportunity to selectively modulate GPCR function in a diverse and rich way.<sup>21</sup> Positive allosteric modulators (PAMs) are able to elevate the natural effect of hormones and endogenous ligands, either by increasing potency or by maximizing efficacy, and may additionally display intrinsic activity (ago-PAMs).<sup>21</sup> Furthermore, PAMs may induce functional selectivity for signaling pathways not inherent to the natural ligand.<sup>21</sup> Another characteristic of allosteric modulators is their saturable effect, which has the potential to fine-tune receptor signaling, as well as minimizing risks such as drug overdosing.<sup>21</sup> Thus, the search for allosteric scaffolds provides a novel opportunity to identify the first orally bioavailable drug candidates modulating SCTRs.

Here, we outline the development of a four-stage testing funnel with the capability to detect, validate, and characterize biologically relevant SCTR small-molecule modulators. Our approach includes the design of a diverse selection of PAM primary screening assays differing not only in their detection method but also in their orthosteric stimulus response, which

have been compared by screening a 12,000-compound small-molecule library. We also established a set of secondary assays to validate and characterize promising scaffolds regarding target engagement and functional selectivity. The results demonstrate how the combination of assays arranged in the testing funnel led to the discovery of the first low-molecular-weight, nonpeptidyl SCTR-specific PAMs.

## Materials and Methods

### Peptides and Ligands

Sec-FL (full-length human secretin [1–27]; cat. 4031250), GLP-1 (GLP-1 trifluoroacetate salt; cat. 4030663), and AVP ([Arg<sup>8</sup>]-vasopressin trifluoroacetate salt; cat. 4012215) were obtained from Bachem AG (Bubendorf, Switzerland). Secretin 1–23 (Sec(1–23); HSDGTFSTSELSRLREGARLQ RLL-OH) and secretin 3–27 (Sec(3–27); DGTFTSELSRLR EGARLQRLQLGLV-NH<sub>2</sub>) were custom synthesized by Biopeptide (San Diego, CA). GLP-1(9–36) (cat. AS-65070) was obtained from Anaspec (Fremont, CA). BETP (4-(3-(benzyloxy)phenyl)-2-(ethylsulfinyl)-6-(trifluoromethyl)pyrimidine) was purchased from Sigma-Aldrich (St. Louis, MO; cat. SML0558; purity ≥98% [high-performance liquid chromatography]).

### Cells and Culture Reagents

Chinese Hamster ovary (CHO-K1) cells and human embryonic kidney (HEK)-293(T) cells were obtained from ATCC (Manassas, VA). CHO-K1 cells were maintained in CHO cell growth media (Ham's F-12K [Kaighn's modification]; Corning Life Sciences, Tewksbury, MA; Cellgro cat. 10-025-CV), 5% fetal bovine serum (FBS) clone II (GE Healthcare Life Sciences, Marlborough, MA; Hyclone cat. SH30066.03), 1% penicillin (10,000 units)/streptomycin (10 mg) (Pen/Strep; Thermo Fisher Scientific, Waltham, MA; Gibco cat. 15140122), and 1% L-glutamine (200 mM; Gibco cat. 25030081). HEK-293(T) cells were maintained in HEK cell growth media (Dulbecco's modified Eagle's medium [DMEM]; Corning Life Sciences; Cellgro cat. 10-013-CV), 10% FBS (Omega Scientific, Tarzana, CA; cat. FB-12), 1% Pen/Strep, and 1% L-glutamine. Cells were detached using TrypLE Express (Gibco; cat. 12605036). Antibiotics used for stable cell selection were Hygromycin B (Omega Scientific; cat. HG-80), G418 (Omega Scientific; cat. GN-04), and Blastidicin (InvivoGen, San Diego, CA; cat. ant-bl-1).

The chemical library was obtained from BioAscent Discovery Ltd. (Newhouse, Lanarkshire, UK), consisting of 12,000 cluster centroids providing diverse representatives of an expanded 125,000 small-molecule compound BioAscent collection. Each of the scaffolds in the expanded library contains 10–30 analogs that help to rapidly validate scaffolds and establish nascent structure–activity relationships (SARs)

through cherry-picked orders of hits and analogs as liquid stocks. The library was stored as 2 mM stocks in 100% DMSO.

All assays were performed at the Conrad Prebys Center for Chemical Genomics (CPCCG) High-Throughput Screening Facility.

### cAMP Accumulation Assays

Cyclic adenosine monophosphate (cAMP) assays were performed using frozen stocks of parental CHO-K1 cells, SCTR- or AVP2R-overexpressing CHO-K1 cells, or GLP-1R-overexpressing HEK-293T cells, all derived from a single cell clone at a low passage number. After reaching 80%–90% confluency, cells were harvested using TrypLE Express, centrifuged, and resuspended in freeze media (10% DMSO in growth media). The final concentration of the cell stocks was 20 million cells/mL. Corresponding ligand standard curves were recorded for each cell batch to obtain adequate EC<sub>20</sub> and EC<sub>95</sub> concentrations.

**General Procedure.** The time-resolved fluorescence resonance energy transfer (TR-FRET)-based cAMP accumulation assays were performed according to the manufacturer's instructions with a few modifications. In brief, orthosteric stimulator dilutions were prepared freshly in DMSO and transferred to Echo Qualified 384-well, low-dead-volume (384LDV) microplates (Labcyte, San Jose, CA) via a CAPP 16-channel pipette (CAPP, Nordhausen, Germany). Compounds and ligands were dispensed onto dry microplates with an Echo liquid handler (Labcyte). The final assay compound concentration was 10  $\mu$ M for primary screening and hit confirmation (in triplicate) or 12.5  $\mu$ M for 1025 hits and analogs (in triplicate). Frozen cell stocks were thawed quickly in a 37 °C water bath and diluted in stimulation buffer (HBSS [Hank's Balanced Salt Solution with Ca<sup>2+</sup> and Mg<sup>2+</sup>]; Gibco; cat. 24020117), 5 mM HEPES (hydroxyethyl piperazineethanesulfonic acid), 0.075% BSA (7.5% DTPA-purified bovine serum albumin; PerkinElmer Inc., Waltham, MA; cat. CR84-100), and 0.5 mM IBMX (3-isobutyl-1-methylxanthine; Sigma-Aldrich; cat. I5879) to obtain the desired cell density. Cells were dispensed using a Multidrop Combi dispenser (Thermo Fisher Scientific), centrifuged at 1000 rpm for 1 min, covered with a lid, and kept at room temperature (RT) for 30 min. cAMP standard dilutions (4-fold, 0–1  $\mu$ M final) were prepared in the stimulation buffer and transferred to designated wells using a CAPP 16-channel pipette. Antifoam SE-15 (0.1%; Sigma-Aldrich; cat. A8582) was added to the cAMP detection buffer, which was subsequently filtered through a 40  $\mu$ m cell strainer. Detection reagents were diluted according to the manufacturer's manual (specific dilutions in supplementary information) and dispensed using a Combi dispenser. The plates were centrifuged at 1000 rpm for 1 min, covered with a lid, and read on a Pherastar Plus microplate reader (BMG

Labtech, Ortenberg, Germany) with the HTRF (homogeneous time-resolved fluorescence) module after 30–60 min at RT. Data were uploaded and analyzed on CBIS (Chemical and Biology Information System software; ChemInnovation Software Inc., San Diego, CA). The EC<sub>20</sub> of the ligand was set as the negative control and EC<sub>95</sub> as the positive control. Further characterization was conducted using the TIBCO Spotfire software (PerkinElmer). Compounds with high fluorescence in the TR-FRET donor (reference) channel in comparison with the negative control wells were eliminated from further studies. Specific procedures are described in the Supplementary Information.

### CRE-Luc2P Reporter Assay

Luciferase reporter assays were performed as described previously<sup>22</sup> with a few modifications. In brief, HEK-293 SCTR CRELuc cells were seeded in two T225 cell culture flasks and grown in HEK cell growth media (DMEM, 10% FBS, 1% Pen/Strep, and 1% L-glutamine). After 2 days, cells were detached using TrypLE Express, resuspended in phosphate-buffered saline (PBS), and centrifuged at 300g for 4 min. The cell pellet was resuspended in DMEM + 10% FBS. A cell suspension of 0.25 million cells/mL was seeded into tissue culture-treated 384-well microplates (Greiner Bio-One small volume 784080) via a Multidrop Combi dispenser at 5  $\mu$ L/well. Plates were centrifuged at 500 rpm for 15 s and incubated overnight at 37 °C and 5% CO<sub>2</sub>. The next day, orthosteric stimulator dilutions were freshly prepared in DMSO (positive control: 156 pM Sec-FL final; negative control and compound wells: 5 pM Sec-FL final) and transferred to Echo Qualified 384LDV microplates via a CAPP 16-channel pipette. Compounds (25 nL/well) and ligands (5 nL/well) were dispensed onto microplates with Labcyte Echo, followed by incubation at 37 °C and 5% CO<sub>2</sub>. The final DMSO concentration was 0.60%. After 4 h, plates and Steady-Glo (Promega, Madison, WI) detection reagent were brought to RT for 15 min. Detection reagent was added via a Multidrop Combi dispenser (5  $\mu$ L/well) and plates were centrifuged at 500 rpm for 15 s. Thereafter, assay plates were kept at RT protected from light for 15 min and luminescence was detected via a ViewLux ultra HTS Microplate Imager (PerkinElmer; 5 s read). Data were uploaded and analyzed using CBIS. The EC<sub>20</sub> of the ligand was set as the negative control and EC<sub>95</sub> as the positive control. Further characterization was conducted via TIBCO Spotfire. Cell line generation and clonal selection of HEK-293 SCTR CRELuc cells are described in the Supplementary Information.

### TR-FRET SNAP-SCTR Binding Assay

Binding experiments were performed as previously described,<sup>23–26</sup> with the following modifications.

Selected compounds A1, A9, B1, C1, and D1 were stored in 384LDV microplates in a desiccator as 16-point twofold dilutions in DMSO. Stock concentrations ranged from 0 to 10 mM. Fluorescein-labeled secretin (Fluo-Sec) and Sec-FL were diluted in DMSO and dispensed into a 384LDV plate. Ligand titrations were prepared in DMSO in adjacent wells. Using Labcyte Echo, Fluo-Sec was transferred (25 nL, 6 nM final) into all test wells of a 1536-well plate (Corning; cat. 3725), DMSO (25 nL, positive control), and Sec-FL (25 nL, 5  $\mu$ M final, negative control) or ligand/compound titrations (25 nL, varying concentrations) were dispensed on top. Using a dounce homogenizer, thawed HEK-293 SNAP-SCTR membranes labeled with Lumi-4 Terbium cryptate (Cisbio Tag-lite) were diluted in binding buffer (10 mM HEPES, pH 7.4, 100 mM NaCl, 10 mM  $MgCl_2$ , 1 mM ascorbic acid, and 0.2% BSA) to a final concentration of 5  $\mu$ g/mL. Membrane solution was added via a Multidrop Combi dispenser at 5  $\mu$ L/well. The plate was centrifuged 1000 rpm for 1 min and incubated at RT for 2 h. Competition binding/allosteric modulator titration was recorded by Pherastar FSX (LanthaScreen 520/490 module). Data were uploaded and analyzed via CBIS as well as via GraphPad Prism 8.4.0 (GraphPad Software Inc., San Diego, CA) by applying the equation “One site – Fit  $K_i$ ” to determine equilibrium dissociation constants  $K_i$  of orthosteric ligands. Allosteric modulators were analyzed using the equation “Allosteric modulator titration” to obtain equilibrium dissociation constants  $K_b$  and cooperativity factors  $\alpha$ .  $\alpha = 1$  indicates neutral cooperativity,  $0 < \alpha < 1$  indicates negative modulation, and  $\alpha > 1$  supports positive cooperativity. Experiments were performed in duplicate in at least three independent experiments. Procedures for cell line generation, clonal selection, and membrane preparation of HEK-293 SNAP-SCTR, as well as for saturation and dissociation binding experiments, are described in the Supplementary Information.

### Calcium Flux Assay with FLIPR Calcium 6 Dye

SCTR-CHO-K1 cells were grown in the CHO cell growth media. After reaching 80%–90% confluency, cells were harvested using TrypLE Express, resuspended in growth media, and seeded into a 384-well plate (5000 cells/50  $\mu$ L/well; Greiner Bio-One; cat. 781091). Plates were covered with lids, centrifuged at 500 rpm for 1 min, and incubated at 37  $^{\circ}$ C and 5%  $CO_2$  overnight. The next day, growth media was removed by an upside-down spin (300 rpm for 5 s). Immediately, 20  $\mu$ L of FLIPR Calcium 6 dye (membrane-permeable  $Ca^{2+}$  indicator; Molecular Devices, San Jose, CA) in assay buffer (HBSS with  $Ca^{2+}$  and  $Mg^{2+}$  containing 20 mM HEPES, 0.1% BSA, and 2.5 mM probenecid [Sigma-Aldrich; cat. P-7861]) was added per well. The plate was centrifuged at 500 rpm 5 s and subsequently incubated at 37  $^{\circ}$ C and 5%  $CO_2$  for 2 h. Test ligand titrations

were prepared on a 384LDV plate and then transferred to a 384-well NBS plate (Non-Binding Surface; Corning; cat. 3655). Assay buffer was added to the compound source plate using a Multidrop Combi dispenser to a final volume of 40  $\mu$ L/well. Cell plates were equilibrated at RT for 30 min. Hamamatsu FDSS 7000 (Functional Drug Screening System; Hamamatsu Photonics, Hamamatsu City, Japan) was used for liquid dispenses and fast kinetic reads. Ten microliters of ligand solution was added to 20  $\mu$ L of cells in dye media while monitoring fluorescence (3 min read, addition at 10th read interval, normal exposure FLUO3/4). All experiments were performed in duplicate in at least three independent experiments. Curve-fitting analysis was conducted by GraphPad Prism 8.4.0.

### NanoBiT $\beta$ -Arrestin-2 Recruitment Assay

$\beta$ -Arrestin-2 recruitment assays were developed and performed as reported previously,<sup>27</sup> with a few modifications.

HEK-293 cells were seeded into a 6-well plate at a cell density of 0.3 M/well and were incubated overnight at 37  $^{\circ}$ C and 5%  $CO_2$ . Following the manufacturer's manual, pFC220K-SCTR-SmBiT and LgBiT-ARRB2, pFC220K-SCTR-SmBiT and ARRB2-LgBiT, or pFC220K-AVP2R-SmBiT and LgBiT-ARRB2 were transfected using TRANSIT-LT1 transfection reagent (Mirusbio, Madison, WI; cat. MIR2300) delivering 0.5  $\mu$ g of DNA of each construct per well. After 24 h, cells were harvested using TrypLE Express, resuspended in growth media, centrifuged at 300g for 3 min, and resuspended in assay buffer (HBSS with  $Mg^{2+}$  and  $Ca^{2+}$ , 5 mM HEPES, 0.1% BSA) to a final cell density of 0.4 million/mL. Cell suspension was dispensed in an AlphaPlate-384 (light gray, shallow well; PerkinElmer; cat. 6008350) using a Multidrop Combi dispenser. After centrifugation at 500 rpm for 15 s, 3  $\mu$ L of NanoBiT detection reagent was added per well via Multidrop Combi. The plate was covered, centrifuged at 1000 rpm for 1 min, and monitored with Pherastar FSX (luminescence, kinetic mode, 0.2 s read) for 2 h or until the baseline appeared to stabilize. Ligand (Sec-FL, Sec(1–23), Sec(3–27), or AVP) titrations were prepared in DMSO in 384LDV plates. Utilizing an Echo liquid dispenser, ligand titrations (40 nL/well) were transferred into cell plates. In the case of characterization of PAMs, DMSO (20 nL) or compound A1 or B1 (20 nL, 12.5  $\mu$ M final) was dispensed into sample wells before Sec-FL titration. The plate was covered and centrifuged at 1000 rpm for 1 min, and  $\beta$ -arrestin-2 recruitment was recorded via Pherastar FSX (luminescence, kinetic mode, 0.2 s read) for 30 min. Experiments were performed in duplicate or triplicate in at least three independent experiments and curves were fitted using GraphPad Prism 8.4.0. Plasmids, construct generation, and the clonal selection of HEK-293 SCTR-SmBiT LgBiT-ARRB2 are described in the Supplementary Information.



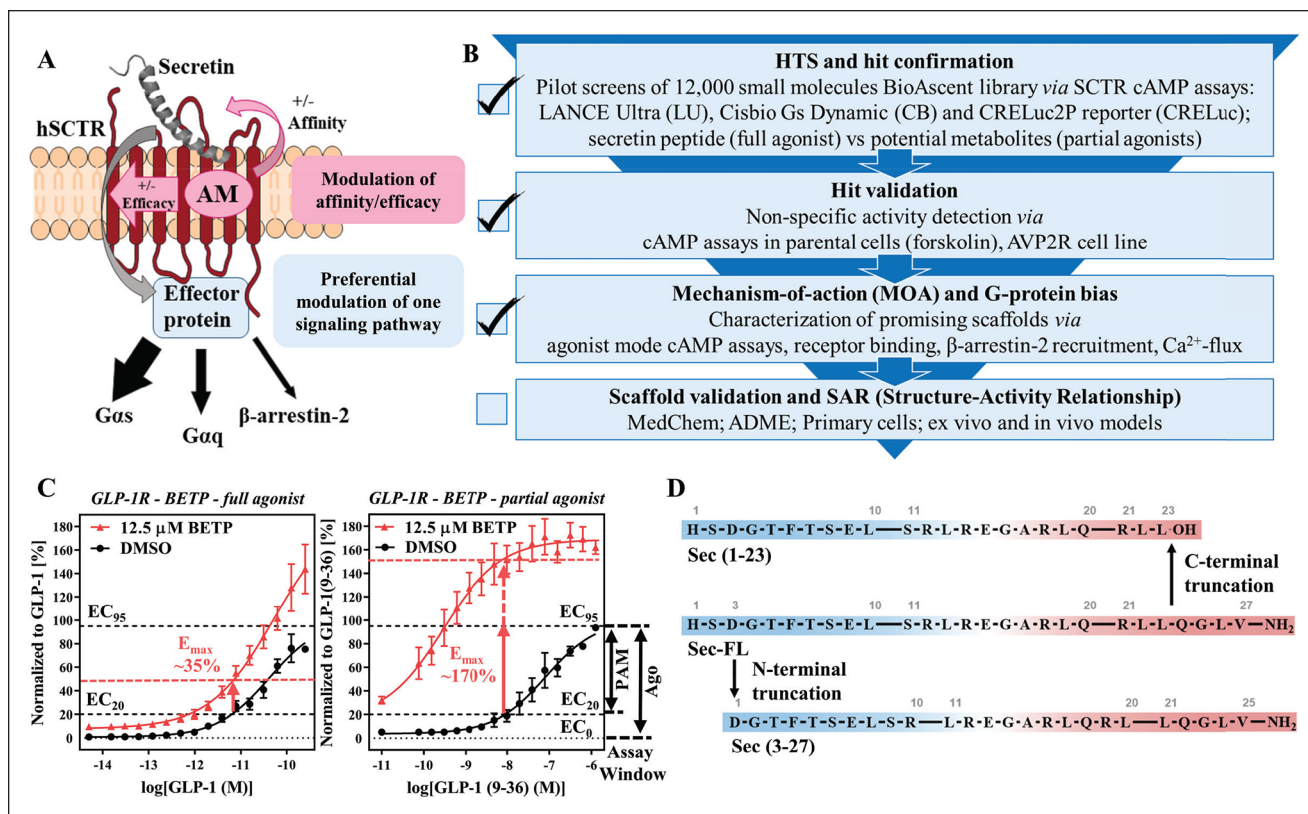


**Figure 1.** Strategies for the development of a testing funnel to detect PAMs targeting SCTRs. **(A)** Advantages of allosteric modulator signaling and display of SCTR signaling pathways (adapted from Ortiz Zacarias et al.<sup>50</sup>). **(B)** Development of biological assays for the establishment of a testing funnel to identify biologically relevant SCTR small-molecule modulators consisting of four levels: HTS and hit confirmation, hit validation, MOA and G protein bias, and scaffold validation and SAR studies. Check marks indicate stages that have been completed successfully. **(C)** GLP-1R PAM BETP<sup>17,33</sup> as a model demonstrating substantial probe dependency and the corresponding effect on cAMP accumulation assay sensitivity. Left panel: DMSO- (black) versus BETP- (12.5  $\mu$ M, red) treated GLP-1 full-length (full-agonist) peptide predicting a primary screening response of around 35%. Right panel: DMSO- (black) versus BETP- (12.5  $\mu$ M, red) treated GLP-1(9–36) (partial agonist) predicting a primary screening response well beyond 100%. TR-FRET ratios (relative fluorescence units) are normalized to the corresponding peptide agonist and plotted using GraphPad Prism; data points are shown as mean  $\pm$  SEM. Depiction of assay windows of the PAM mode (negative control: EC<sub>20</sub>; positive control: EC<sub>95</sub> of ligand) and agonist mode (negative control: no ligand; positive control: EC<sub>95</sub> of ligand), which served as the basis of SCTR screening assays. **(D)** Secretin and its truncated analogs mimicking potential metabolites of secretin (from top down): Sec(1–23), product of C-terminal truncation (carboxylic acid [–OH]); Sec-FL (full-length, amide [–NH<sub>2</sub>]), endogenous peptide acting on SCTRs; and Sec(3–27) amide, product of N-terminal truncation.

## Results

### Development of a Four-Stage Testing Funnel to Detect PAMs Targeting SCTRs

To enhance our chances for discovering orally bioavailable drug candidates targeting SCTRs, we focused our efforts on the identification of PAMs, which may not only potentiate the effect of secretin and related peptides, but also selectively channel activation of signaling pathways (Fig. 1A). We fortified our drug discovery program by developing a panel of diverse assays that build four essential stages for our screening campaign. Starting with high-throughput screening (HTS) and hit confirmation (Fig. 1B), it was our

aim to develop a robust and efficient primary screening assay based on G $\alpha$ s protein signaling, which represents the dominant physiological effect upon SCTR activation and leads to increased cAMP levels. It is well known in the HTS field that different assays detecting the same cellular processes would inadvertently produce distinct sets of hits; some of them may be enhanced by the detection approach used in the assay, while others may be enhanced by unique settings specific to each of these assays.<sup>28</sup> Therefore, we compared three different cAMP detection methods (PerkinElmer LANCE Ultra, Cisbio Gs Dynamic [Cisbio GsD], and Promega CRELuc2P reporter [CRELuc] technology<sup>22</sup>) by performing pilot screens of a small-molecule

library consisting of 12,000 compounds. Since PAMs may display reduced or no activity without an orthosteric ligand present,<sup>29–31</sup> we developed PAM screening assays using a fixed concentration ( $EC_{10}$  to  $EC_{20}$ ; based on TR-FRET ratios or relative luminescence units [RLUs]) of agonist as the basal orthosteric stimulator response in compound and negative control wells. Since PAM assays are able to detect both PAMs and (allosteric) agonists, we additionally characterized compounds in agonist mode assays performed in the absence of peptide ligands to determine their intrinsic activity. The  $EC_{95}$  concentration of the peptide agonist served as a positive control in both cases. Similar approaches have been described for recent PAM screening efforts against other GPCRs.<sup>20,32</sup>

Beyond that, we evaluated the screening efficiency comparing full agonists and partial agonists. This was based on the observation of substantial probe dependency of GLP-1R PAMs, such as BETP,<sup>17,33</sup> toward the partial agonist GLP-1(9–36), which is generated via N-terminal truncation of GLP-1 by DPP4 (dipeptidyl-peptidase-4).<sup>34</sup> **Figure 1C** illustrates benefits of using a partial agonist in the PAM assay. The extent of response from BETP in the presence of the  $EC_{20}$  concentration of GLP-1 (**Fig. 1C**, left panel) is significantly lower than that observed with the partial agonist GLP-1(9–36) (**Fig. 1C**, right panel). Intriguingly, BETP would be considered a weak hit with a 35% response using the full agonist as the basal stimulator, but would reach activity well beyond 100% when used with the partial agonist. Inspired by this increase of sensitivity, we explored potential secretin peptide metabolites. Sec-FL, like other peptide hormones, is known to be metabolized and cleared rapidly (half-life of ~2–4 min<sup>8</sup>). Although there is no clear description of physiologic Sec-FL degradation products, we mimicked metabolites after known truncated versions of endogenous ligands targeting other class B GPCRs, which could serve as useful tools to evaluate the assay sensitivity and probe dependency of potential PAMs. For example, Sec-FL was shown to be degraded by NEP (neutral endopeptidase) 24.11, but no specific cleavage products were reported.<sup>35</sup> Another in vitro study suggested the formation of Sec(1–23) (**Fig. 1D**, top) by VIP-degrading endoprotease through C-terminal cleavage of Sec-FL (**Fig. 1D**, middle).<sup>36</sup> To explore effects of C- and N-terminal truncation of Sec-FL, we acquired Sec(1–23) and Sec(3–27) (**Fig. 1D**, bottom). In stage 2 of our testing funnel (**Fig. 1B**) we validated hits by eliminating nonspecific activators. To that end, we translated our developed cAMP detection methods to cell lines not expressing SCTRs, such as parental cells and type 2 arginine vasopressin receptor (AVP2R)-bearing cells. AVP2R was selected, since it also couples to  $G_{\alpha s}$  proteins while exerting physiologic effects contradictory to SCTR activation.<sup>37</sup> Besides being a class A GPCR, AVP2R should not be affected by SCTR targeting hits.

### Development of Secondary Assays to Enable Broader Scaffold Validation and Compound Profiling

To strengthen our ability to validate and profile promising scaffolds regarding their mechanism of action (MOA), we developed and optimized secondary assays to evaluate the target engagement and functional selectivity of potential PAMs. Inspired by previously reported TR-FRET-based binding assays,<sup>23,24,38</sup> we inserted a SNAP-tag to the N-domain of SCTR and created stably expressing HEK-293 cell clones. The construct was compared with a wildtype (WT) receptor by monitoring the agonist response in cAMP accumulation assays to ensure functional integrity (**Suppl. Fig. S1C**). Additionally, we introduced a fluorescein molecule to the C-terminal end of Sec-FL via a diethylene glycol linker presenting a lysine residue (**Suppl. Fig. S1A**). Of note, the absence of basic amino acids in the sequence of secretin enabled the use of lysine instead of an oxidation-sensitive cysteine residue to attach the probe. cAMP accumulation experiments in CHO-SCTR cells confirmed that the introduction of the fluorescein tag did not hamper agonist activity (**Suppl. Fig. S1B**). Being assured our constructs maintained WT-like biological behavior, we prepared membranes of Lumi4-Tb- (Lumi-4 terbium cryptate, Cisbio Tag-lite) labeled SNAP-SCTR cell clones. Depending on the assay format, membranes were incubated with Fluo-Sec, in addition to orthosteric or allosteric ligands, resulting in TR-FRET signaling that can be quantified to assess the fraction of Fluo-Sec bound to SNAP-SCTR (**Fig. 2A**). To determine the dissociation constant ( $K_d$ ), saturation binding experiments were performed (**Fig. 2B**), which served as the basis to conduct further experiments like competition binding (**Figs. 2C and 3B**; see **Fig. 6C**) and dissociation binding assays (see **Fig. 6D**). Intriguingly, the homogeneous format, simplicity, and lack of radioactivity allow time-dependent measurements in a high-throughput format with minimal use of resources (time, ligand, compounds, plates, etc.), in contrast to standard radioisotope binding assays.

Since functional selectivity has been shown to provide potential therapeutic benefits relevant for GPCRs,<sup>39–43</sup> we designed a  $\beta$ -arrestin-2 recruitment assay applying Promega's NanoBiT technology.<sup>44</sup> As reported in a similar study on cannabinoid receptors,<sup>30</sup> we made use of an 11-amino acid peptide (Small BiT [SmBiT]) attached to the C-terminal end of the GPCR and the 17.6 kDa Large BiT (LgBiT) tag introduced either on the N- or C-terminal end of  $\beta$ -arrestin-2 (ARRB2). To validate our procedure, we generated and tested constructs for SCTR and AVP2R (**Suppl. Fig. S2**). The latter served as a control described by Promega's brochure for NanoBiT technology. Upon agonist activation, GPCRs get phosphorylated, followed by  $\beta$ -arrestin-2 recruitment. This event leads to complementation of the inactive SmBiT and LgBiT subunits, resulting in a

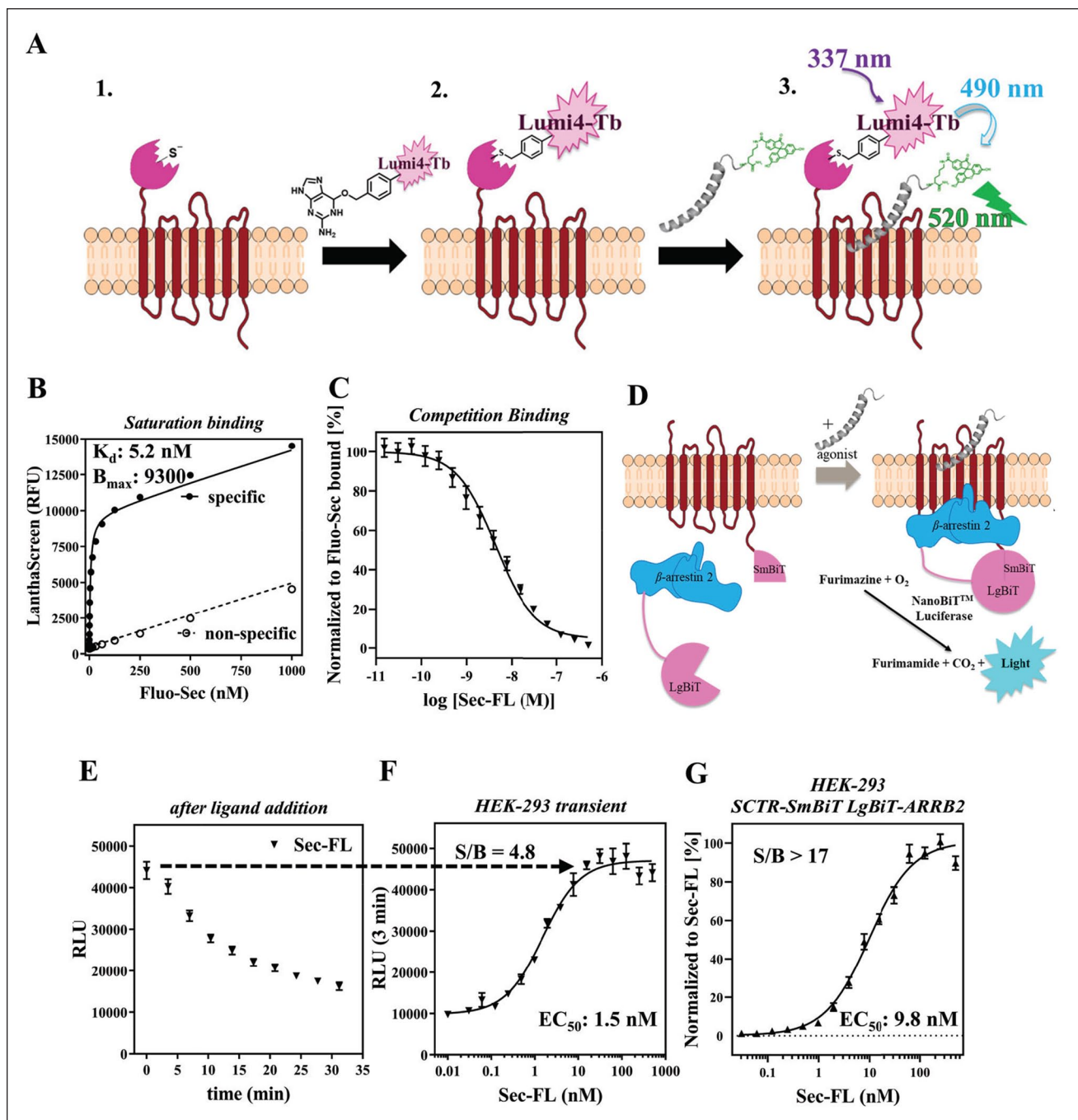


**Figure 2.** Development of GPCR-specific secondary assays to enable immediate scaffold validation and compound characterization. **(A)** Design and mechanism of TR-FRET-based binding assay employing SNAP-tag technology and Fluo-Sec. **(B)** Saturation binding curve of Fluo-Sec determining dissociation constant  $K_d$ . **(C)** Competition binding curve of Sec-FL; LanthasScreen ratios are normalized to Fluo-Sec bound to SNAP-SCTRs. **(D)** Design and mechanism of  $\beta$ -arrestin-2 recruitment assay exploiting NanoBiT (Promega) technology. **(E)** Real-time luminescence after ligand addition to evaluate the best time point for an endpoint read. **(F)** Dose-response curve of Sec-FL at 3 min (transiently expressing HEK-293 cells). **(G)** Normalized dose-response curve of Sec-FL (HEK-293 SCTR-SmBiT LgBiT-ARRB2 cell clone,  $n = 4$ ); raw data S/B ratio more than 17. RLU are normalized to Sec-FL; graphs were plotted using GraphPad Prism; data points are shown as mean  $\pm$  SEM.



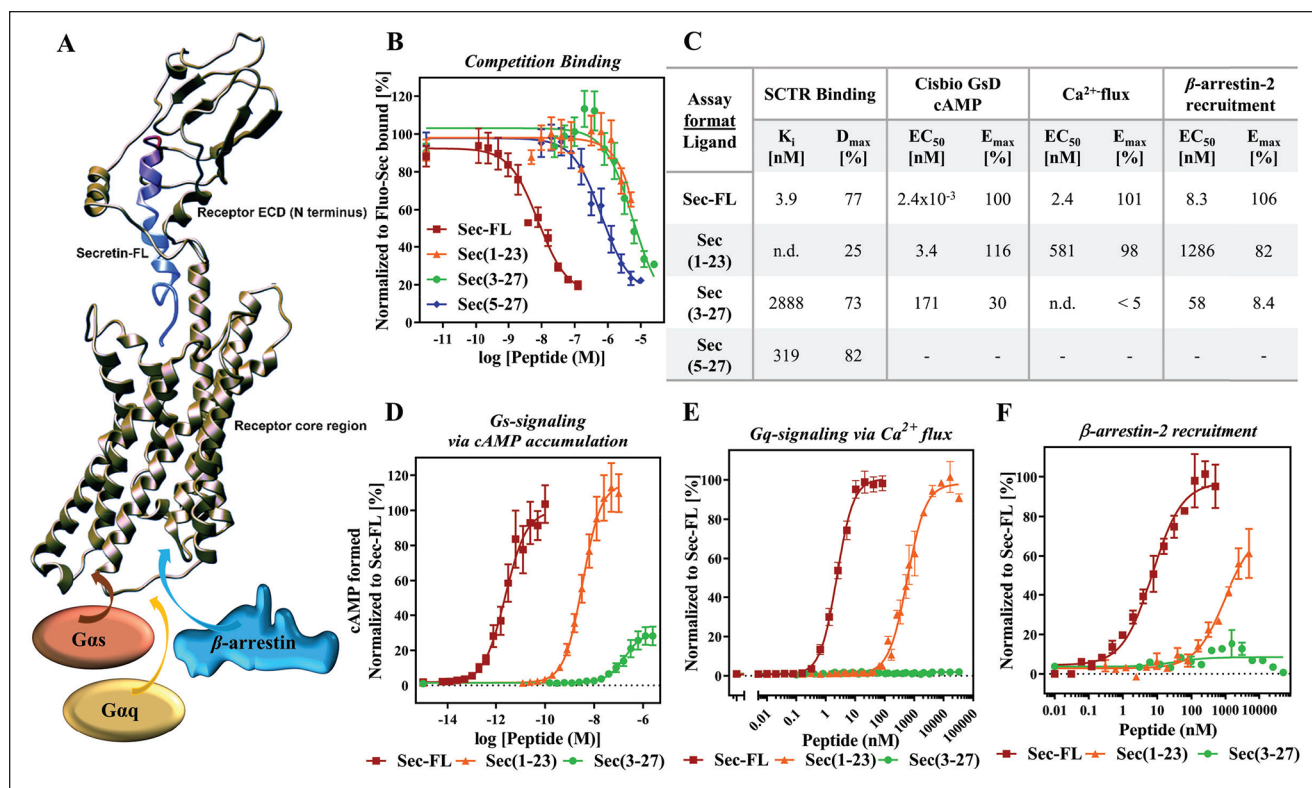


**Figure 3.** C-terminal truncation of secretin leads to a low-affinity, low-potency but fully efficacious agonist, whereas N-terminal cleavage drastically reduces efficacy among investigated signaling pathways. **(A)** 3D model of secretin bound to SCTR (adopted from Miller et al.<sup>45</sup>) with illustration of two peptide binding sites: C-terminal end of secretin (red) binding to a receptor N-domain (also known as ECD) and N-terminal tail of secretin (blue) positioning in a receptor core helical bundle. Upon secretin binding, effector proteins are recruited, including *Gas* and *Gαq* proteins as well as β-arrestin. **(B)** Competition binding of Fluo-Sec with secretin and truncated analogs—Sec-FL (red), Sec(1–23) (orange), Sec(3–27) (green), and Sec(5–27) (blue)—to determine binding affinities  $K_i$  [nM] and fractions displaced ( $D_{max}$  [%]). Lanthascreen ratios are normalized to Fluo-Sec bound to SNAP-SCTRs. **(C)** Summary of affinities, potencies, and efficacies of Sec-FL analogs in performed assays in table format. Activity of Sec-FL (red), Sec(1–23) (orange), and Sec(3–27) (green) inducing **(D)** cAMP accumulation, **(E)** Ca<sup>2+</sup> flux, and **(F)** β-arrestin-2 recruitment. **(D)** TR-FRET ratios converted to cAMP concentrations [nM], **(E)** cytosolic Ca<sup>2+</sup> F/F<sub>0</sub> ratio, and **(F)** RLU. **(D–F)** Normalized to Sec-FL. Graphs were plotted using GraphPad Prism; experiments were performed in duplicate or triplicate. **(B, D, E)** Combined and **(F)** representative graphs of three independent experiments; data points are shown as mean ± SEM.

luminescent signal by restoring the catalytic activity of the very bright NanoLuc luciferase (**Fig. 2D**). The engagement of GPCR and β-arrestin-2 can be monitored in real time, revealing the best suitable time point for endpoint reads. As described by Promega, addition of AVP resulted in a sustained luminescence signal peaking after about 10 min (**Suppl. Fig. S2B, C**). Interestingly, in the case of HEK-293 cells expressing SCTR-SmBiT and LgBiT-ARRB2, the luminescence signal peak occurs immediately upon Sec-FL addition, decreasing steadily over time (**Fig. 2E**). Therefore, we chose to analyze concentration–response curves after 3 min of ligand addition (**Fig. 2F**). In transiently overexpressing HEK-293 cells, dose–response was recorded with a signal-to-background (S/B) ratio of 4.8 (**Suppl. Fig. S2D**), while the selection of a single cell clone expressing SCTR-SmBiT and LgBiT-ARRB2 constructs improved the S/B ratio to more than 17 (**Fig. 2G**). Of note, co-transfection of

SCTR-SmBiT with ARRB2-LgBiT resulted in a similar kinetic profile but more than 10-fold lower RLU; hence, it was the less favorable option for assay optimization (**Suppl. Fig. S2B**).

### C-Terminal Cleavage of Secretin Leads to Low-Affinity, Low-Potency, but Fully Efficacious Agonist, whereas N-Terminal Truncation Drastically Reduces Efficacy among Investigated Signaling Pathways

After establishing a strong panel of assays, we validated the developed assays by characterizing our truncated secretin analogs Sec(1–23) and Sec(3–27). Several examples in recent studies revealed a two-site binding mode of hormones to class B GPCRs, which is also depicted in **Figure 3A**, illustrating a



three-dimensional (3D) model<sup>45</sup> of secretin-bound SCTR. As shown previously,<sup>14,45,46</sup> the C-terminal end of secretin peptide binds tightly to the large extracellular domain (ECD) of the receptor while directing the N-terminal end of secretin toward the helical core bundle, inducing intramolecular arrangements that lead to the activation of effector proteins, such as G $\alpha$ s and G $\alpha$ q proteins or  $\beta$ -arrestins. Considering this binding model, we were not surprised that compared with Sec-FL (red,  $K_i$  = 3.9 nM), Sec(1–23) (orange,  $K_i$  not determined) suffered from a slightly greater loss of affinity than Sec(3–27) (green,  $K_i$  = 2.9  $\mu$ M). Interestingly, further cleavage of the N-terminal tail resulting in Sec(5–27) led to higher binding affinity ( $K_i$  = 319 nM) compared with other truncated analogs (Fig. 3B,C). In agreement with the 3D model, Sec(1–23) displays up to a 3-log loss of potency (cAMP formed  $EC_{50}$  = 3.4 nM, Ca<sup>2+</sup> flux  $EC_{50}$  = 581 nM,  $\beta$ -arrestin-2  $EC_{50}$  = 1.3  $\mu$ M) compared with Sec-FL (cAMP formed  $EC_{50}$  = 2.4 pM, Ca<sup>2+</sup> flux  $EC_{50}$  = 2.4 nM,  $\beta$ -arrestin-2  $EC_{50}$  = 8.3 nM) but retains full efficacy among performed functional assays (Fig. 3D–F). Sec(3–27) displayed additional loss of potency (cAMP formed  $EC_{50}$  = 171 nM) and significantly decreased efficacy ( $E_{max}$  = 30%) in cAMP accumulation assays while lacking any activity in experiments investigating Ca<sup>2+</sup> flux or  $\beta$ -arrestin-2 recruitment. This dramatic loss of function due to two missing amino acids at the N-terminal end of the natural peptide is consistent with the two-site binding model and with reports on other class B GPCRs.<sup>32</sup> Of note, the inability of Sec(3–27) to induce a G $\alpha$ q-mediated response or  $\beta$ -arrestin-2 recruitment might indicate a potential bias toward G $\alpha$ s signaling that we plan to investigate further in future studies.

### Stage 1.1: Pilot Screen of BioAscent Library Using LANCE Ultra cAMP Assay Revealed Probe Dependency of Hits Toward Secretin or Its Truncated Forms

Our screening efforts began with a pilot screen utilizing the PerkinElmer LANCE Ultra cAMP detection kit (Fig. 4A) against the 12,000-compound BioAscent library at a 10  $\mu$ M concentration. Deploying Sec-FL as the orthosteric basal stimulator in PAM mode, we obtained 361 hits (3% hit rate). Hit confirmation studies ( $EC_{20}$  Sec-FL, 10  $\mu$ M compound in triplicate) led to 106 confirmed hits. Purchase of these 106 hits and 919 analogs (5–15 analogs/scaffold, 1025 compounds total), selected to provide a nascent SAR for identified hits as liquid stocks from BioAscent and subsequent evaluation in hit confirmation format ( $EC_{20}$  Sec-FL, 10  $\mu$ M compound in triplicate), yielded 368 hits (90 reconfirmed original hits and 278 active analogs). Eleven of these hits were eliminated by screening in parental CHO-K1 cells using the same detection method. To investigate the effects of the truncated secretin analogs, we performed in parallel three screens of 1025 hits and analogs in the PAM format with either Sec-FL,

Sec(1–23), or Sec(3–27) as the orthosteric basal stimulator ( $EC_{20}$  for each peptide). These efforts resulted in a pool of 34 confirmed hits, and by elucidating the chemical structures we were able to identify five common scaffolds (scaffolds A–E). In-depth analysis of 34 confirmed hits via scatterplot and pie chart (Fig. 4B) revealed a probe dependency of the hits toward certain peptides. Two of 34 molecules have been confirmed with all three secretin analogs, whereas 30 hits were obtained from screens with individual peptides. The pie chart illustrates the distribution of scaffolds among the individual peptides and indicates that scaffolds B and E could be found by employing either one of the peptides, whereas the confirmation of scaffolds A, C, and D was dependent on the orthosteric stimulator applied. It should be pointed out that scaffolds A, B, and C have related chemical structures, mainly differing from their  $R^2$  substituents at the pyrimidine ring (Fig. 4C), strengthening their credibility as hits. While implementing and performing these assays, we observed high day-to-day variability in the detected level of stimulation with the same concentration of agonist. For example, screening the same compound set of 1025 hits and analogs in the Sec-FL PAM mode resulted in two very different hit rates, 368 hits in the first run (indicated as squares in the scatterplot) and 21 hits in the second run. After in-depth attempts to troubleshoot, we established that minor experimental variances in cell density and the concentration of the agonist resulted in a disproportionately high variation of signal due to the high slope of the standard curve, resulting in a narrow dynamic range. We addressed this issue by comparing calibration curves of cAMP detected by either the LANCE Ultra or Cisbio GsD cAMP kit (Fig. 4D), which is advertised to perform with a greater dynamic range. The assay dynamic range was determined by a cAMP concentration range between  $IC_{10}$  and  $IC_{90}$  of the standard curve. Indeed, in contrast to LANCE Ultra (slope  $\sim$  1.5; dynamic range = 0.18–3.52 nM cAMP), the CisBio GsD detection kit demonstrated a slope close to unity and a much broader dynamic range (slope  $\sim$  0.9; dynamic range = 0.22–38.2 nM cAMP). Greater sensitivity and a steeper slope were also observed in the dose–response curves of secretin peptides detected with the LANCE Ultra cAMP kit (Fig. 4E). We decided that the small dynamic range of the LANCE Ultra kit is a major drawback for performing larger screens in the PAM mode, since it is crucial to ensure consistent baseline stimulation.

### Stage 1.2: Pilot Screens Comparing Three Different Detection Methods and Two Sets of Ligand Probes Elucidate the Strength of Combining Sec-FL, Sec(1–23), and Sec(3–27) as the Orthosteric Stimulator

To explore further primary screening options, we tested the 12,000-compound BioAscent collection in three further

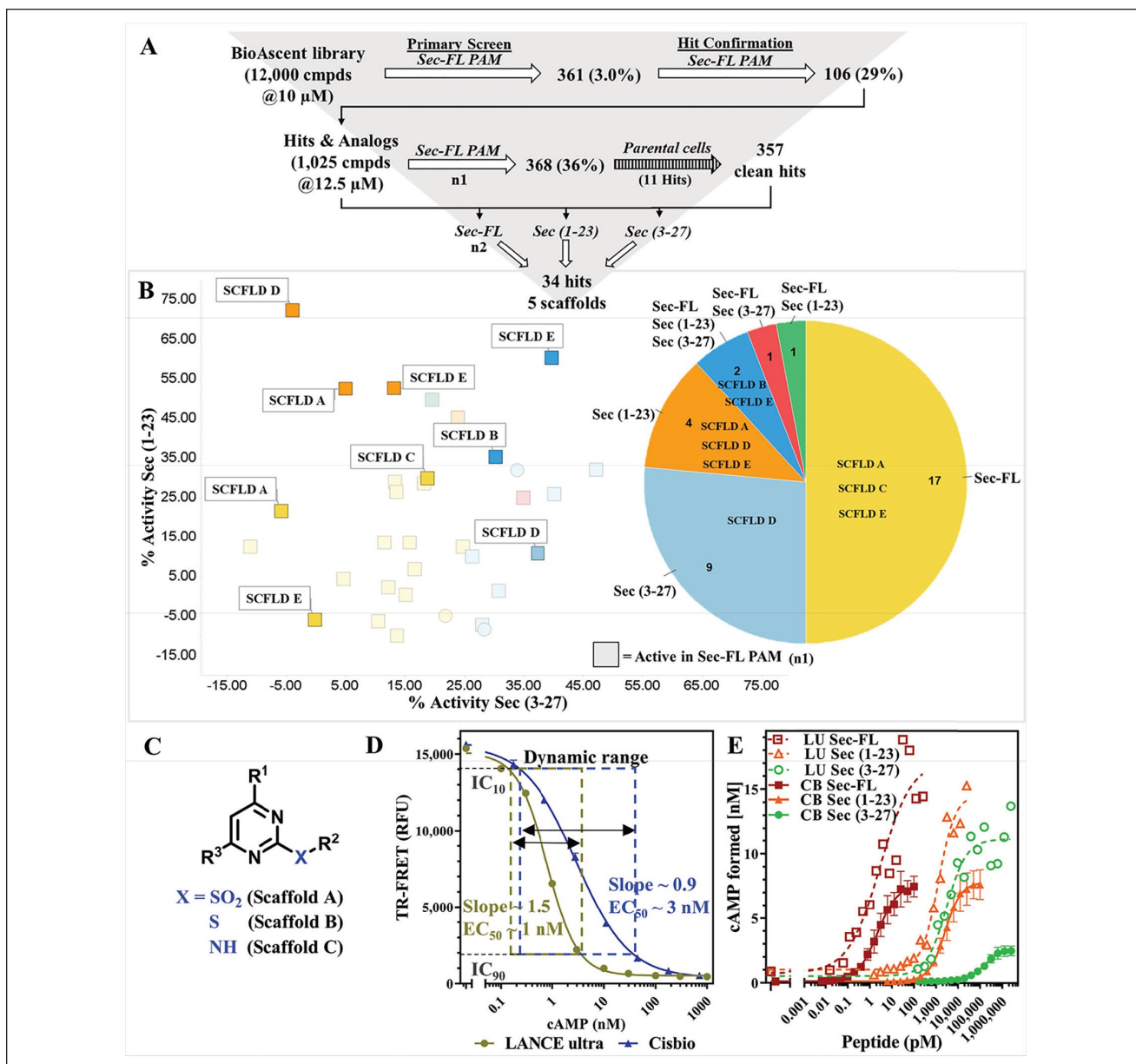


**Figure 4.** Pilot screen of BioAscent library employing the LANCE Ultra cAMP assay revealed the probe dependency of hits toward secretin or its truncated forms. **(A)** Pilot screen of BioAscent library using the LANCE Ultra cAMP kit and an EC<sub>20</sub> of Sec-FL as the stimulant. The primary screen and hit confirmation yielded 106 hits; 1025 liquid stocks comprising hits and corresponding analogs were purchased and subsequently validated in the primary assay. A counterscreen with parental cells eliminated 11 compounds; 1025 hits and analogs were screened with individual secretin peptides, yielding 34 hits and 5 prevalent scaffolds. **(B)** Breakdown of 34 hits into six groups: confirmed hit by Sec-FL (yellow,  $n = 17$ ), Sec(3–27) (light blue,  $n = 9$ ), Sec(1–23) (orange,  $n = 4$ ), all three peptides (dark blue,  $n = 2$ ), Sec-FL and Sec(3–27) (red,  $n = 1$ ), or Sec-FL & Sec(1–23) (green,  $n = 1$ ). Scatterplot showing percent activity with Sec(3–27) ( $x$  axis) in correlation to percent activity with Sec(1–23) ( $y$  axis). The squares indicate hit confirmation in the first round of the screen with Sec-FL; the pie chart depicts the fraction of hits and detected scaffolds per peptide/peptide mixture. The scatterplot and pie chart were created using TIBCO Spotfire. **(C)** Scaffolds A–C contain closely related chemical structures. **(D)** Comparison of cAMP standard curves using the LANCE Ultra (beige) or Cisbio GsD (blue) detection kit confirmed a lower sensitivity but broader dynamic range for Cisbio GsD cAMP detection. The assay dynamic range was determined by IC<sub>10</sub> to IC<sub>90</sub> of the cAMP standard curve: LANCE Ultra 0.18–3.52 nM cAMP; Cisbio GsD 0.22–38.2 nM cAMP. **(E)** cAMP formation of secretin analogs applying LANCE Ultra (dotted lines) compared with Cisbio GsD (solid lines) technology: Sec-FL (red), Sec(1–23) (orange), and especially Sec(3–27) (green) demonstrate greater responsiveness but lower reproducibility with LANCE Ultra (LANCE Ultra is representative of three experiments; Cisbio GsD combined the results of three experiments). Graphs were plotted using GraphPad Prism; data points are shown as mean  $\pm$  SEM.

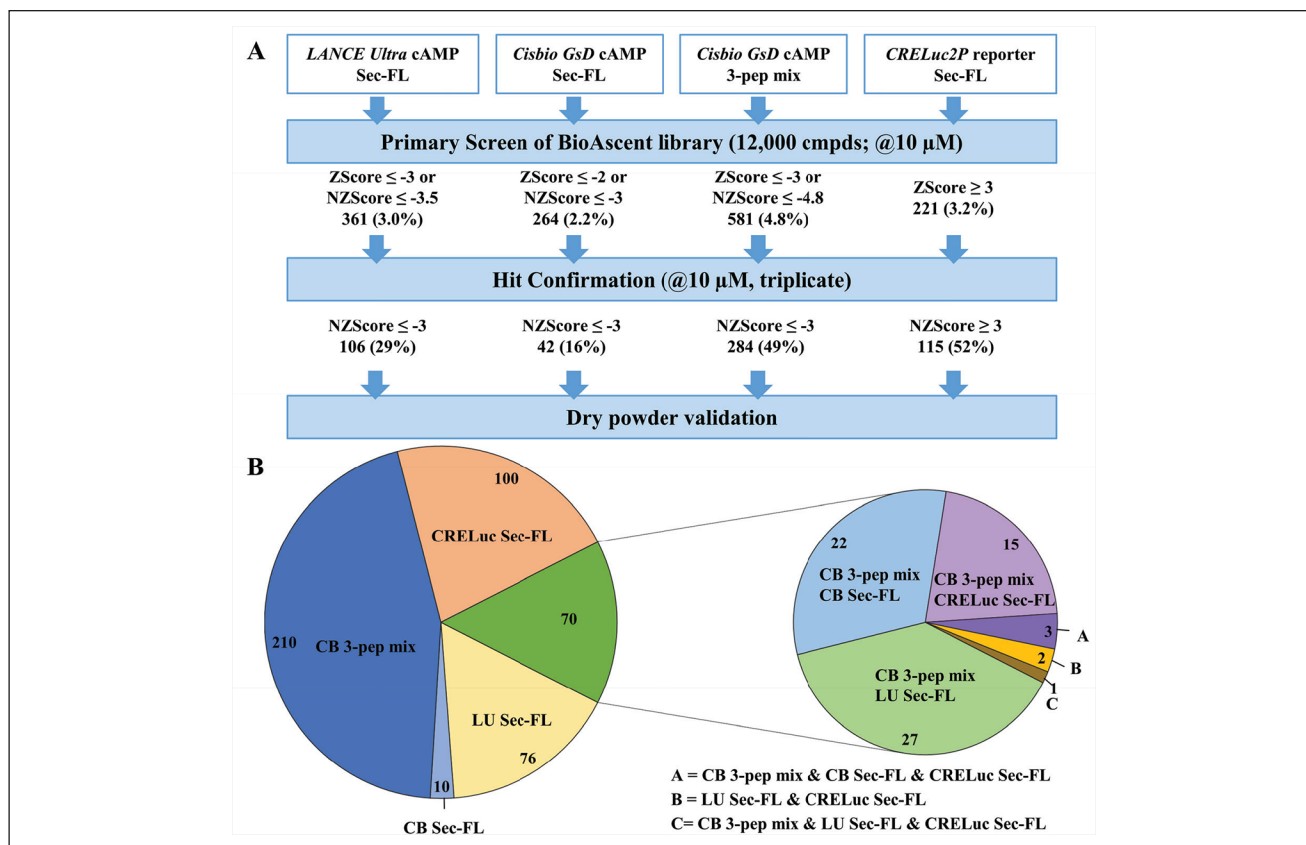


**Figure 5.** Pilot screens comparing three different detection methods and two sets of ligand probes elucidate the strength of combining Sec-FL, Sec(1–23), and Sec(3–27), that is, the 3-peptide mix as the orthosteric stimulator. **(A)** Pilot screens using LANCE Ultra cAMP (stimulant EC<sub>20</sub> Sec-FL), Cisbio GsD Sec-FL (stimulant EC<sub>20</sub> Sec-FL), Cisbio GsD 3-peptide mix (stimulant EC<sub>10</sub> Sec-FL, Sec(1–23), and Sec(3–27)), or CRELuc (stimulant EC<sub>10</sub> Sec-FL) technologies. Hit confirmation criteria of an NZ of score  $\geq 3$  ( $\leq -3$ ) were applied to all four formats. **(B)** Pie chart breaking down the total confirmed hits ( $n = 466$ ), confirmed via LANCE Ultra (light yellow, 76), Cisbio GsD Sec-FL (light blue, 10), Cisbio GsD 3-peptide mix (dark blue, 210), CRELuc (light orange, 100), or multiple assays (green, 70), whereby 68 of 70 compounds were confirmed by the Cisbio GsD 3-peptide mix. Pie chart created using Microsoft Excel.

formats (**Fig. 5A**). Taking into account the probe dependency and potentially increased sensitivity for stimulating with truncated peptides, we decided to perform in parallel a screen with full agonist Sec-FL and a screen with a mixture of EC<sub>10</sub> concentrations of all three peptides (3-peptide mix), which resulted in a basal stimulation comparable to EC<sub>20</sub> of Sec-FL alone. To obtain better reproducibility and a greater dynamic range, we used the Cisbio GsD cAMP kit as the detection method. We were also interested in applying a technology that is distinct from TR-FRET detection of intracellular cAMP. Hence, we selected the CRELuc system with a luminescence-based detection system for our third pilot screen employing Sec-FL as the basal stimulator. All four methods performed well in the primary screen, having decent to good Z' factors (0.54–0.61) and reasonable S/B ratios (**Suppl. Table S1**). We utilized the Z score for the selection of hits in primary HTS with slightly different cutoff criteria for each assay to obtain a similar number of hits. Selecting hits using the Z score is not optimal for hit confirmation studies; thus,

we employed an NZ score of ( $-$ ) 3 as the cutoff criteria to compare the four screening assays in the hit confirmation stage (**Fig. 5A**). The NZ score is calculated as the difference between the sample mean and the mean of the negative control divided by the standard deviation of the negative control wells in the plate. Hits demonstrate negative NZ scores in loss-of-signal cAMP TR-FRET assays and positive NZ scores in gain-of-signal CRELuc assays. In total, 466 hits were confirmed. Comparing the three detection methods using Sec-FL as the orthosteric stimulator, we found that CRELuc confirmed the highest number of hits ( $n = 115$ ), followed by LANCE Ultra with 113 hits. In contrast, Cisbio GsD was only able to confirm 42 hits when Sec-FL was deployed as the agonist, probably due to the lower sensitivity of this detection kit. However, the 3-peptide mix Cisbio GsD assay outnumbered the other three detection methods by confirming 284 hits, which indicates significantly increased assay sensitivity by utilizing a mixture of full and partial agonists. We created a pie chart depicting the fractions of



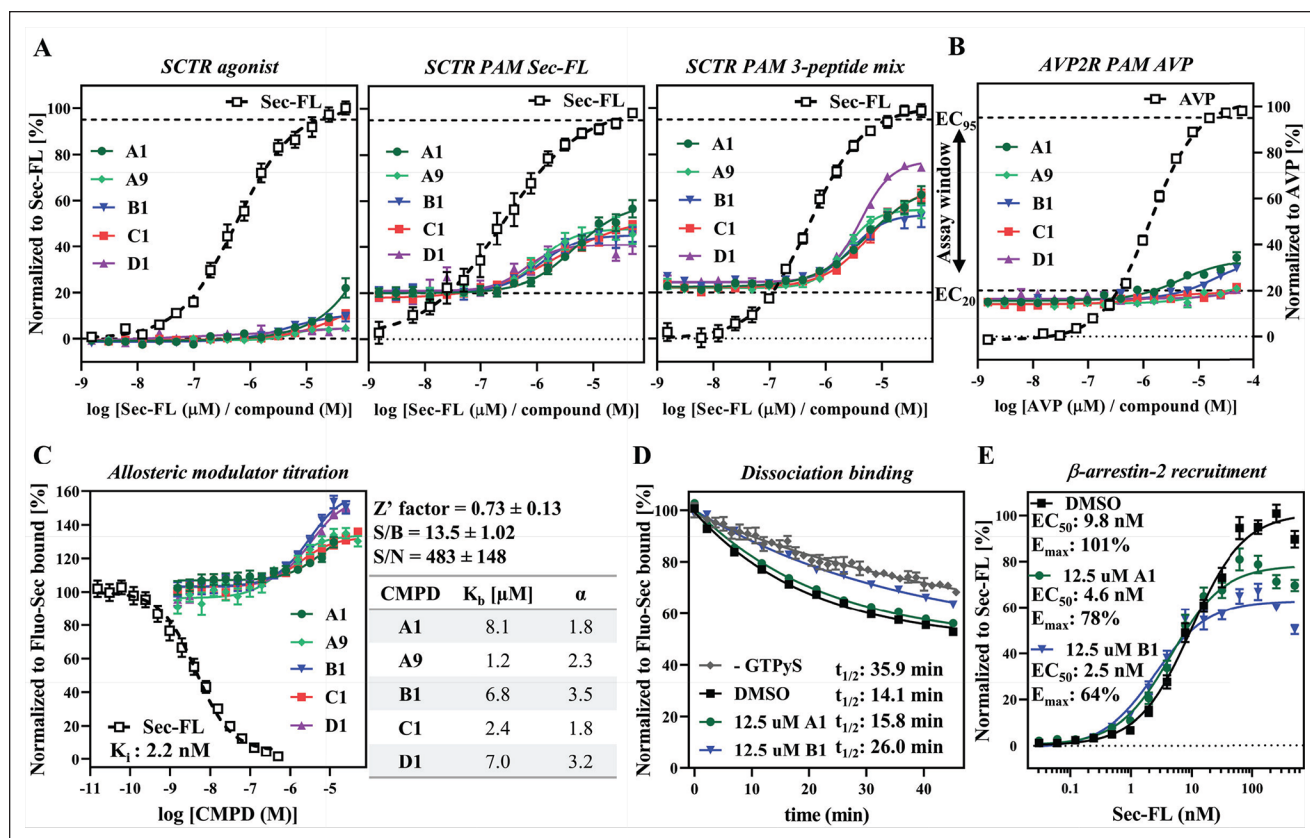


**Figure 6.** Validation and characterization of scaffold. (**A–D**, left to right) Compound titration on (**A**) SCTR-bearing CHO-K1 cells detected by Cisbio GsD agonist (no stimulant), Cisbio GsD Sec-FL (stimulant  $EC_{20}$  Sec-FL), and Cisbio GsD 3-peptide mix (stimulant  $EC_{10}$  Sec-FL, Sec(1–23), and Sec(3–27)) or on (**B**) AVP2R-expressing CHO-K1 cells via Cisbio GsD kit (stimulant  $EC_{20}$  AVP). (**C**) Allosteric modulator titration using TR-FRET binding assay in high-throughput mode (assay performance data right of graph) and subsequent analysis in GraphPad Prism yielding allosteric activity parameters  $K_b$  (equilibrium dissociation constant of PAM) and  $\alpha$  (cooperativity factor). (**D**) Compound B1 demonstrating effect on Fluo-Sec dissociation comparable to presence of G protein (–GTP $\gamma$ S). (**E**) Compounds A1 and B1 slightly enhance potency but diminish efficacy of Sec-FL for recruitment of  $\beta$ -arrestin-2. (**A,B**) TR-FRET ratios resulting from cAMP accumulation normalized to full agonist. (**C,D**) LanthaScreen ratios are normalized to Fluo-Sec bound or (**E**) RLU normalized to Sec-FL. (**A–E**) Compounds A1 (dark green), A9 (light green), B1 (blue), C1 (red), and D1 (purple). Graphs were plotted using GraphPad Prism; experiments were performed in duplicate or triplicate in at least three independent experiments; data points are shown as mean  $\pm$  SEM.

compounds found in individual assays as well as compounds that have been detected in more than one assay (Fig. 5B, left pie chart). We further analyzed the 70 hits confirmed in multiple assays by assigning them to their originating method (Fig. 5B, right pie chart). Intriguingly, 68 of the 70 compounds were hits confirmed by the Cisbio GsD 3-peptide mix, whereas only 21 of the overlapping hits derived from the CRELuc screening. A closer look into activities of overlapping hits via scatterplot revealed two molecules (scaffolds A and D) that had been detected by individual peptide screening with LANCE Ultra detection (Suppl. Fig. S3).

### Stages 2 and 3: Molecules with Scaffolds A–D Are SCTR-Selective PAMs

Moving into stages 2 and 3 of our testing funnel (Fig. 1B), we purchased dry powders of 110 compounds for hit

validation. In the course of this study, we focused on two compounds (A1 and A9) containing scaffold A; two compounds (B1 and C1) with closely related structures, scaffold B and C, respectively; and one compound (D1) incorporating scaffold D. To explore intrinsic activity, we recorded dose–response curves in SCTR-CHO cells in the agonist mode (Fig. 6A, left panel). In this setting, we detected negligible activity for compounds A1, B1, and C1. Performing the same assay except stimulating cells with an  $EC_{20}$  concentration of Sec-FL (Fig. 6A, middle panel), we were able to measure dose–response curves for all five compounds with potencies in the single-digit micromolar range and efficacies ranging from 20% (D1, purple) to 40% (A1, dark green) (Suppl. Tables S2 and S3). We then utilized the 3-peptide mix as an orthosteric stimulator (Fig. 6A, right panel), which led to similar ranges in potencies and efficacies for compounds with scaffold A (e.g., 44% for

compound A1 [dark green]) but a significantly higher response in the case of compound D1 (purple, 53%), indicating probe dependency. To evaluate nonspecific activities, we performed the same assay in AVP2R-expressing CHO-K1 cells and AVP as the stimulating agent (Fig. 6B). Compared with their PAM activity on SCTRs, compounds A1 (dark green) and B1 (blue) demonstrated negligible activity in the AVPR2 PAM assay. For further discrimination of their allosteric activity, we studied compounds in newly developed secondary assays.

Binding assays are useful tools not only to dissect orthosteric from allosteric ligands but also to determine allosteric activity parameters.<sup>14</sup> In a competition binding-type experiment we detected a dose-dependent increase of Fluo-Sec binding for all five compounds supporting an allosteric binding site on SCTRs (Fig. 6C, Suppl. Table S3). The experiment was carried out in a 1536-well plate—thus consistent with HTS—and demonstrated robust behavior with a  $Z'$  factor of 0.73 and S/B ratio around 13.5. The data were subjected to an allosteric modulator titration analysis, which generated equilibrium dissociation constants  $K_b$  and cooperativity factors  $\alpha$  for each compound (Fig. 6C, table). Similar to potencies in cAMP assays, the  $K_b$  values were within the micromolar range. Interestingly, compounds B1 (blue) and D1 (purple) displayed the highest cooperativity to Fluo-Sec, with  $\alpha$  values of 3.5 and 3.2, respectively. The best tool to distinguish between orthosteric and allosteric binders is a dissociation binding experiment (Fig. 6D).<sup>47</sup> To accelerate Fluo-Sec dissociation, we added GTP $\gamma$ S to our dissociation buffer, which is known to shift the equilibrium of receptors into the G protein-uncoupled state and thereby attenuate agonist binding.<sup>48</sup> The addition of 12.5  $\mu$ M compound A1 (dark green) only slightly decelerated Fluo-Sec dissociation, whereas an equal concentration of compound B1 (blue) was able to slow down dissociation of Fluo-Sec comparable to the presence of G proteins (minus GTP $\gamma$ S, gray). Beyond that, we tested compounds A1 (dark green) and B1 (blue) regarding their PAM activity for Sec-FL-stimulated  $\beta$ -arrestin-2 recruitment (Fig. 6E). Both compounds slightly enhanced potency but attenuated efficacy of Sec-FL to recruit  $\beta$ -arrestin-2.

## Discussion

### *Comparison of Methods Reveals Key Features for a Successful Screen to Identify PAMs*

Here we report the development and results of a testing funnel that incorporates a structured comprehensive toolbox to identify, validate, and characterize low-molecular-weight nonpeptidyl SCTR modulators. To date, no other small-molecule compounds have been described to interact with SCTRs. Hence, it was crucial to develop and select a robust and global primary screening method. By comparing not

only three different detection methods (LANCE Ultra, Cisbio GsD, and CRELuc), but also the effect of individual as well as mixed full and partial peptide agonists deployed as orthosteric basal stimulators, we were able to evaluate the most critical aspects for successful implementation of an SCTR PAM screening assay based on pilot screens comprising 12,000 compounds. Our goal was to establish a primary screening assay with great sensitivity, reproducibility, and hit detection range. Initial efforts were conducted applying LANCE Ultra cAMP technology stimulating with Sec-FL. While demonstrating great assay sensitivity and good assay performance in the 1-day primary screen, the approach suffered from a lack of day-to-day reproducibility, likely due to a narrow dynamic range of the detection kit. Hence, we decided to test orthogonal approaches relying on intracellular cAMP accumulation, such as Cisbio GsD and CRELuc detection systems. Despite having a broader dynamic range, the Sec-FL Cisbio GsD assay demonstrated lower assay sensitivity, which led to a significant reduction in the number of confirmed hits. Utilizing the luminescence-based CRELuc reporter system resulted in a higher assay sensitivity, an improved S/B ratio, and a higher number of hits. These factors, beyond the lower cost of detection reagents, make it attractive for large-scale HTS campaigns. However, the overlap of CRELuc-derived hits and hits confirmed by TR-FRET-based methods was only around 30%, indicating substantial differences in the nature of hits.

### *Novel Application of 3-Peptide Mix Results in Higher Assay Sensitivity and Allows Identification of SCTR PAMs with Distinct Probe Dependencies*

The profiling of 1025 hits and analogs via LANCE Ultra cAMP employing Sec-FL or truncated secretin peptides Sec(1–23) and Sec(3–27) revealed that the response of potential PAMs is dependent on the nature of the orthosteric stimulator. Although this phenomenon has already been described for PAMs acting on other GPCRs,<sup>33</sup> there is no such pattern described for SCTRs. This might be due to the poorly understood metabolism of Sec-FL, which might vary depending on its site of expression. However, potential secretin metabolites are likely to be cleavage products from either end of the full-length peptide; thus, we focused our studies on one analog truncated at the C-terminal tail<sup>36</sup> (Sec(1–23)) and one analog designed as a hypothetical N-terminal degradation product (Sec(3–27)). Due to the development of a comprehensive set of SCTR binding and functional assays, we were able to thoroughly characterize our metabolite models, revealing that C-terminal peptide truncation leads to a lower affinity, but fully functional analog, whereas N-terminal cleavage results in an analog exerting only partial SCTR activation. These distinct activity

profiles in combination with the modification of receptor occupancy and restricted binding space can be utilized to increase the sensitivity and effectiveness of PAM screening assays.<sup>32</sup> Looking ahead, PAMs able to enhance activity of truncated partially active versions of Sec-FL might be particularly useful for therapeutic applications by extending the functional response of the natural ligand after its degradation and inactivation.<sup>20,30,32</sup> Our studies with individual secretin peptides in the LANCE Ultra PAM screening assay elucidated that each peptide finds distinct sets of compounds. Since the nature of physiological metabolites remains unclear, we decided to combine all three analogs into one orthosteric stimulator probe (3-peptide mix) to identify PAMs that are likely to work with any potential metabolite. Due to the broader dynamic range, we employed the Cisbio GsD detection kit to conduct the screen of the BioAscent library in 3-peptide mix format. The primary screen worked well with a good  $Z'$  factor and decent S/B ratio of around 3. Moreover, Cisbio GsD 3-peptide mix was not only able to identify the largest number of hits but also empowered to detect 97% of overlapping hits, which were found utilizing Sec-FL in LANCE Ultra, Cisbio GsD, or CRELuc assays. Hence, the Cisbio GsD 3-peptide mix assay is a robust, reproducible, sensitive, and effective primary screening assay.

### ***Secondary Assays Reveal That Identified Scaffolds Exert Different MOAs***

The pool of overlapping hits provided five interesting scaffolds, four of which were investigated in detail. Dry powders of compounds A1, A9, B1, C1, and D1 were validated in dose–response studies on SCTRs regarding their ability to accumulate cAMP with no orthosteric ligand, Sec-FL, or 3-peptide mix basal stimulation. In general, compounds showed no to marginal intrinsic activity in agonist mode, but significant responses in PAM modes. Intriguingly, compounds A1 and A9 demonstrated comparable activities in both Sec-FL and 3-peptide mix cAMP assays, whereas compound D1 exerted greater effects with mixed agonists, therefore suggesting distinct MOAs. Compounds A1 and B1 appeared to produce slight responses in CHO-AVP2R cells stimulated with AVP; however, compound B1 displayed 18-fold selectivity toward SCTRs. Of note, structural analog A9 was inactive in the AVP2R-PAM cAMP assay, proposing that specificity is achievable through structural modification. The development of a fluorescence-based target engagement assay enabled the characterization of compounds on SCTR binding in a high-throughput environment. We were excited to see that all five compounds were able to increase Fluo-Sec binding in a dose-dependent manner. Resulting cooperativity factors  $\alpha$  revealed further subtle differences between investigated scaffolds. Compound A1 displayed lower  $\alpha$  values in

the allosteric modulator titration and only slightly decreased Fluo-Sec dissociation rates in SNAP-SCTR dissociation binding experiments. However, compound B1, exhibiting stronger positive cooperativity to Fluo-Sec, was able to exert comparable deceleration of Fluo-Sec dissociation-like coupled G proteins, the most widely studied endogenous PAM targeting GPCRs. To explore potential signaling bias, we also subjected compounds A1 and B1 to Sec-FL-stimulated  $\beta$ -arrestin-2 recruitment studies. Both compounds reduced efficacy but were able to slightly enhance Sec-FL potency. Whether this phenomenon is due to functional selectivity of PAMs or a nonspecific interaction with the assay will be addressed in future studies.

### ***Testing Funnel Identifies the First Small-Molecule Modulators Described for SCTRs***

The combination of a diverse selection of primary screens, intensive comparison of their primary screen performance, design of GPCR-specific secondary assays, and consequential arrangement of funnel stages resulted in the discovery of PAMs targeting SCTRs. One of the main novelties of our testing funnel was the development of the 3-peptide mix stimulator that not only substantially enhanced assay sensitivity and effectiveness but also allowed the detection of probe-dependent hits. Another unique advantage was the development and implementation of GPCR-specific secondary assays, which led to immediate profiling and validation of distinct sets of hits with respect to target engagement and functional selectivity. This is the first report, to our knowledge, describing small-molecular-weight compounds that not only interact with SCTRs but also significantly enhance the binding and response of secretin peptides. Encouragingly, discovered hits cover effects on both natural peptide ligand and metabolite models, considerably increasing chances for potential therapeutic application.

### ***Future Directions: Testing Funnel Stage 4***

In this study we discovered bona fide SCTR PAM hits. We continue working with identified scaffolds in further hit validation and optimization studies by extending structural variety through analog-by-catalog and medicinal chemistry efforts. Like many HTS-suitable cell-based assays, the use of receptor overexpressing cell lines may result in overly amplified or distorted signaling. Thus, hits will be confirmed using cell models with endogenous SCTR expression and signaling. Hit-to-lead studies involving further optimization of MOA, pharmacokinetics, and toxicity profiles are expected to identify analogs suitable for in vivo testing. Beyond that, future work will include the expansion of GPCR selectivity screens not only to detect possible



off-target effects but also to explore the potential of class B GPCR polypharmacology,<sup>49</sup> which might provide additional benefits for the treatment of metabolic disorders.

## Acknowledgments

We would like to thank personnel of the Conrad Prebys Center for Chemical Genomics (CPCCG) at the Sanford Burnham Prebys Medical Discovery Institute (SBP) for help in diverse aspects of this project.

## Declaration of Conflicting Interests

The authors declared no potential conflicts of interest with respect to the research, authorship, and/or publication of this article.

## Funding

The authors disclosed receipt of the following financial support for the research, authorship, and/or publication of this article: We acknowledge support from the U.S. National Institutes of Health (NIH) National Heart, Lung, and Blood Institute (NHLBI) grant R01HL133501.

## References

1. Bayliss, W. M.; Starling, E. H. The Mechanism of Pancreatic Secretion. *J. Physiol.* **1902**, *28*, 325–353.
2. Ishihara, T.; Nakamura, S.; Kaziro, Y.; et al. Molecular Cloning and Expression of a cDNA Encoding the Secretin Receptor. *EMBO J.* **1991**, *10*, 1635–1641.
3. de Graaf, C.; Song, G.; Cao, C.; et al. Extending the Structural View of Class B GPCRs. *Trends Biochem. Sci.* **2017**, *42*, 946–960.
4. Afroze, S.; Meng, F.; Jensen, K.; et al. The Physiological Roles of Secretin and Its Receptor. *Ann. Transl. Med.* **2013**, *1*, 29.
5. Grossini, E.; Molinari, C.; Morsanuto, V.; et al. Intracoronary Secretin Increases Cardiac Perfusion and Function in Anaesthetized Pigs through Pathways Involving Beta-Adrenoceptors and Nitric Oxide. *Exp. Physiol.* **2013**, *98*, 973–987.
6. Li, Y.; Schnabl, K.; Gabler, S.-M.; et al. Secretin-Activated Brown Fat Mediates Prandial Thermogenesis to Induce Satiety. *Cell* **2018**, *175*, 1561–1574.e12.
7. Modvig, I. M.; Andersen, D. B.; Grunddal, K. V.; et al. Secretin Release after Roux-en-Y Gastric Bypass Reveals a Population of Glucose-Sensitive S Cells in Distal Small Intestine. *Int. J. Obes. (Lond)* **2020**. DOI: 10.1038/s41366-020-0541-7.
8. Brandler, J.; Miller, L. J.; Wang, X. J.; et al. Secretin Effects on Gastric Functions, Hormones and Symptoms in Functional Dyspepsia and Health: Randomized Crossover Trial. *Am. J. Physiol. Gastrointest. Liver. Physiol.* **2020**, *318*, G635–G645.
9. van Witteloostuijn, S. B.; Dalboge, L. S.; Hansen, G.; et al. GUB06-046, a Novel Secretin/Glucagon-Like Peptide 1 Co-Agonist, Decreases Food Intake, Improves Glycemic Control, and Preserves Beta Cell Mass in Diabetic Mice. *J. Pept. Sci.* **2017**, *23*, 845–854.
10. Wu, N.; Meng, F.; Invernizzi, P.; et al. The Secretin/Secretin Receptor Axis Modulates Liver Fibrosis through Changes in Transforming Growth Factor-Beta1 Biliary Secretion in Mice. *Hepatology* **2016**, *64*, 865–879.
11. Singh, K.; Senthil, V.; Arokiaraj, A. W.; et al. Structure-Activity Relationship Studies of N- and C-Terminally Modified Secretin Analogs for the Human Secretin Receptor. *PLoS One* **2016**, *11*, e0149359.
12. Chey, W. Y.; Chang, T. M. Secretin, 100 Years Later. *J. Gastroenterol.* **2003**, *38*, 1025–1035.
13. Imamura, M.; Takahashi, K.; Adachi, H.; et al. Usefulness of Selective Arterial Secretin Injection Test for Localization of Gastrinoma in the Zollinger-Ellison Syndrome. *Ann. Surg.* **1987**, *205*, 230–239.
14. Hoare, S. R. J. Allosteric Modulators of Class B G-Protein-Coupled Receptors. *Curr. Neuropharmacol.* **2007**, *5*, 168–179.
15. Morris, L. C.; Nance, K. D.; Gentry, P. R.; et al. Discovery of (S)-2-Cyclopentyl-N-((1-Isopropylpyrrolidin-2-yl)-9-Methyl-1-oxo-2,9-dihydro-1H-pyrido[3,4-b]indole-4-Carboxamide (VU0453379): A Novel, CNS Penetrant Glucagon-Like Peptide 1 Receptor (GLP-1R) Positive Allosteric Modulator (PAM). *J. Med. Chem.* **2014**, *57*, 10192–10197.
16. Knudsen, L. B.; Kiel, D.; Teng, M.; et al. Small-Molecule Agonists for the Glucagon-Like Peptide 1 Receptor. *Proc. Natl. Acad. Sci. U.S.A.* **2007**, *104*, 937–942.
17. Sloop, K. W.; Willard, F. S.; Brenner, M. B.; et al. Novel Small Molecule Glucagon-Like Peptide-1 Receptor Agonist Stimulates Insulin Secretion in Rodents and from Human Islets. *Diabetes* **2010**, *59*, 3099–3107.
18. King, K.; Lin, N. P.; Cheng, Y. H.; et al. Isolation of Positive Modulator of Glucagon-Like Peptide-1 Signaling from *Trigonella foenum-graecum* (Fenugreek) Seed. *J. Biol. Chem.* **2015**, *290*, 26235–26248.
19. Bueno, A. B.; Showalter, A. D.; Wainscott, D. B.; et al. Positive Allosteric Modulation of the Glucagon-Like Peptide-1 Receptor by Diverse Electrophiles. *J. Biol. Chem.* **2016**, *291*, 10700–10715.
20. Morris, L. C.; Days, E. L.; Turney, M.; et al. A Duplexed High-Throughput Screen to Identify Allosteric Modulators of the Glucagon-Like Peptide 1 and Glucagon Receptors. *J. Biomol. Screen.* **2014**, *19*, 847–858.
21. Congreve, M.; Oswald, C.; Marshall, F. H. Applying Structure-Based Drug Design Approaches to Allosteric Modulators of GPCRs. *Trends Pharmacol. Sci.* **2017**, *38*, 837–847.
22. Cheng, Z.; Garvin, D.; Paguio, A.; et al. Luciferase Reporter Assay System for Deciphering GPCR Pathways. *Curr. Chem. Genom.* **2010**, *4*, 84–91.
23. Emami-Nemini, A.; Roux, T.; Leblay, M.; et al. Time-Resolved Fluorescence Ligand Binding for G Protein-Coupled Receptors. *Nat. Protoc.* **2013**, *8*, 1307–1320.
24. Senthil, V.; Leprince, J.; Vaudry, D.; et al. Fluorescence Resonance Energy Transfer Competitive Binding Assay for Secretin Receptor (Class B-GPCR). *J. Pharm. Pharmacol.* **2014**, *2*, 295–303.
25. Sykes, D. A.; Moore, H.; Stott, L.; et al. Extrapyramidal Side Effects of Antipsychotics Are Linked to Their Association Kinetics at Dopamine D2 Receptors. *Nat. Commun.* **2017**, *8*, 763.
26. Sykes, D. A.; Stoddart, L. A.; Kilpatrick, L. E.; et al. Binding Kinetics of Ligands Acting at GPCRs. *Mol. Cell. Endocrinol.* **2019**, *485*, 9–19.

27. Caninaert, A.; Storme, J.; Franz, F.; et al. Detection and Activity Profiling of Synthetic Cannabinoids and Their Metabolites with a Newly Developed Bioassay. *Anal. Chem.* **2016**, *88*, 11476–11485.
28. Sills, M. A.; Weiss, D.; Pham, Q.; et al. Comparison of Assay Technologies for a Tyrosine Kinase Assay Generates Different Results in High Throughput Screening. *J. Biomol. Screen.* **2002**, *7*, 191–214.
29. Laprairie, R. B.; Kulkarni, P. M.; Deschamps, J. R.; et al. Enantiospecific Allosteric Modulation of Cannabinoid 1 Receptor. *ACS Chem. Neurosci.* **2017**, *8*, 1188–1203.
30. Wootten, D.; Savage, E. E.; Valant, C.; et al. Allosteric Modulation of Endogenous Metabolites as an Avenue for Drug Discovery. *Mol. Pharmacol.* **2012**, *82*, 281–290.
31. Kenakin, T. The Quantitative Characterization of Functional Allosteric Effects. *Curr. Protoc. Pharmacol.* **2017**, *76*, 9.22.1–9.22.10.
32. Nakane, A.; Gotoh, Y.; Ichihara, J.; et al. New Screening Strategy and Analysis for Identification of Allosteric Modulators for Glucagon-Like Peptide-1 Receptor Using GLP-1 (9–36) Amide. *Anal. Biochem.* **2015**, *491*, 23–30.
33. Nolte, W. M.; Fortin, J. P.; Stevens, B. D.; et al. A Potentiator of Orthosteric Ligand Activity at GLP-1R Acts via Covalent Modification. *Nat. Chem. Biol.* **2014**, *10*, 629–631.
34. Mulvihill, E. E.; Drucker, D. J. Pharmacology, Physiology, and Mechanisms of Action of Dipeptidyl Peptidase-4 Inhibitors. *Endocr. Rev.* **2014**, *35*, 992–1019.
35. Hupe-Sodmann, K.; McGregor, G. P.; Bridenbaugh, R.; et al. Characterisation of the Processing by Human Neutral Endopeptidase 24.11 of GLP-1(7–36) Amide and Comparison of the Substrate Specificity of the Enzyme for Other Glucagon-Like Peptides. *Regul. Pept.* **1995**, *58*, 149–156.
36. Gwang-Ho Jeohn, K. T. Purification and Characterization of a Vasoactive Intestinal Polypeptide-Degrading Endoprotease from Porcine Antral Mucosal Membranes. *J. Biol. Chem.* **1995**, *270*, 7809–7815.
37. Juul, K. V.; Bichet, D. G.; Nielsen, S.; et al. The Physiological and Pathophysiological Functions of Renal and Extrarenal Vasopressin V2 Receptors. *Am. J. Physiol. Renal Physiol.* **2014**, *306*, F931–F940.
38. Cottet, M.; Faklaris, O.; Zwier, J. M.; et al. Original Fluorescent Ligand-Based Assays Open New Perspectives in G-Protein Coupled Receptor Drug Screening. *Pharmaceuticals* **2011**, *4*, 202–214.
39. Kenakin, T.; Barker, E. L. Biased Receptor Signaling in Drug Discovery. *Pharmacol. Rev.* **2019**, *71*, 267–315.
40. Manglik, A.; Lin, H.; Aryal, D. K.; et al. Structure-Based Discovery of Opioid Analgesics with Reduced Side Effects. *Nature* **2016**, *537*, 185–190.
41. Gurevich, V. V.; Gurevich, E. V. Biased GPCR Signaling: Possible Mechanisms and Inherent Limitations. *Pharmacol. Ther.* **2020**, *211*, 107540.
42. Bermudez, M.; Nguyen, T. N.; Omieczynski, C.; et al. Strategies for the Discovery of Biased GPCR Ligands. *Drug Discov. Today* **2019**, *24*, 1031–1037.
43. Ilter, M.; Mansoor, S.; Sensoy, O. Utilization of Biased G Protein-Coupled Receptor Signaling towards Development of Safer and Personalized Therapeutics. *Molecules* **2019**, *24*, **2052**.
44. Dixon, A. S.; Schwinn, M. K.; Hall, M. P.; et al. NanoLuc Complementation Reporter Optimized for Accurate Measurement of Protein Interactions in Cells. *ACS Chem. Biol.* **2016**, *11*, 400–408.
45. Miller, L. J.; Dong, M.; Harikumar, K. G. Ligand Binding and Activation of the Secretin Receptor, a Prototypic Family B G Protein-Coupled Receptor. *Br. J. Pharmacol.* **2012**, *166*, 18–26.
46. Dong, M.; Koole, C.; Wootten, D.; et al. Structural and Functional Insights into the Juxtamembranous Amino-Terminal Tail and Extracellular Loop Regions of Class B GPCRs. *Br. J. Pharmacol.* **2014**, *171*, 1085–1101.
47. Klein, M. T.; Vinson, P. N.; Niswender, C. M. Approaches for Probing Allosteric Interactions at 7 Transmembrane Spanning Receptors. *Prog. Mol. Biol. Transl. Sci.* **2013**, *115*, 1–59.
48. DeVree, B. T.; Mahoney, J. P.; Velez-Ruiz, G. A.; et al. Allosteric Coupling from G Protein to the Agonist-Binding Pocket in GPCRs. *Nature* **2016**, *535*, 182–186.
49. Sloop, K. W.; Briere, D. A.; Emmerson, P. J.; et al. Beyond Glucagon-Like Peptide-1: Is G-Protein Coupled Receptor Polypharmacology the Path Forward to Treating Metabolic Diseases? *ACS Pharmacol. Transl. Sci.* **2018**, *1*, 3–11.
50. Ortiz Zacarias, N. V.; Lenselink, E. B.; AP, I. J.; et al. Intracellular Receptor Modulation: Novel Approach to Target GPCRs. *Trends Pharmacol. Sci.* **2018**, *39*, 547–559.